ACS Medicinal Chemistry Letters

Open Access

pubs.acs.org/acsmedchemlett

Letter

Discovery of Non-Covalent Inhibitors for SARS-CoV-2 PLpro: Integrating Virtual Screening, Synthesis, and Experimental Validation

Bruna K. P. Sousa,[¶] Melina Mottin,[¶] Donald Seanego,[¶] Christopher D. Jurisch, Beatriz S. A. Rodrigues, Verônica L. S. da Silva, Milene Aparecida Andrade, Gilberto S. Morais Junior, Diogo F. Boerin, Thamires Q. Froes, Flávia Nader Motta, M. Cristina Nonato, Izabela D. M. Bastos, Kelly Chibale, Richard K. Gessner, and Carolina Horta Andrade*

Cite This: https://doi.org/10.1021/acsmedchemlett.4c00420

Read Online

ACCESS | Metrics & More | Article Recommendations | Supporting Information

ABSTRACT: The SARS-CoV-2 pandemic has significantly challenged global public health, highlighting the need for effective therapeutic options. This study focuses on the papain-like protease (PLpro) of SARS-CoV-2, which is a critical enzyme for viral polyprotein processing, maturation, and immune evasion. We employed a combined approach that began with computational models in a virtual screening campaign, prioritizing compounds from our in-house chemical library against PLpro. Out of 81 virtual hits evaluated through enzymatic and biophysical assays, we identified a modest inhibitor featuring a naphthyridine core with an IC_{50} of 73.61 μM and a K_i of 22 μM. Expanding our exploration, we synthesized and assessed 30 naphthyridine analogues, three of which emerged as promising noncovalent, nonpeptidomimetic inhibitors with IC_{50} values between 15.06 and 51.81 μM. Furthermore, *in vitro* ADMET assays revealed these compounds to possess moderate aqueous solubility, low cytotoxicity, and high microsomal stability, making them excellent candidates for further development targeting SARS-CoV-2 PLpro.

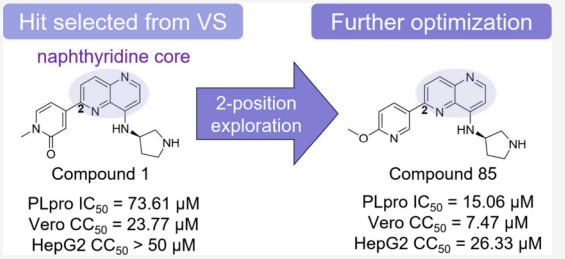

KEYWORDS: *SARS-CoV-2, COVID-19, papain-like protease (PLpro), virtual screening, synthesis, enzymatic assay, noncovalent inhibitor, naphthyridine*

Since the pandemic declaration by the World Health Organization in 2020, the SARS-CoV-2 virus, responsible for severe acute respiratory syndrome (COVID), has caused over 280 million cases and approximately 6 million deaths worldwide.[1] Despite the development and administration of vaccines,[2] the emergence of new variants resistant to these vaccines has raised concerns, which warrant the search for effective therapeutics against the virus.[3]

The current antiviral therapies focus on essential targets for the virus's life cycle. Progress in the development of drugs targeting the main protease (Mpro) or 3C-like protease (3CLpro), such as paxlovid (nirmatrelvir/ritonavir),[4] and the viral polymerase, such as remdesivir[5−8] and molnupiravir,[5,6] has offered a rapid treatment avenue. However, the challenges presented by viral mutations and drug resistance underscore the necessity for alternative strategies.[7] In this regard, the papain-like protease (PLpro), which is conserved across various coronaviruses, plays a critical role in viral replication and immune evasion.[8,9] Unlike highly mutable proteins such as the spike protein, PLpro's conservation among SARS-CoV-2 variants positions it is a promising target for small-molecule inhibitors. Its essential function also diminishes the likelihood of resistance developing due to mutations that would compromise the enzyme's activity.[10] The catalytic site of PLpro cleaves a common motif, LXGG/X, present in nonstructural proteins NSP1/2, NSP2/3, and NSP3/4 proteins. This motif is critical for viral transcription and replication. Moreover, PLpro binding loop 2 (BL-2 Loop) controls access to the active site and is considered the binding site for the noncovalent inhibitor.[8,11] The *N*-terminal ubiquitin-like domain of PLpro also acts as an antagonist to the innate immune pathway, playing a significant role in evading the host immune system.[9] Numerous PLpro inhibitors have been documented in the literature,[11−15] including the compound GRL0617[16] (naphthalene scaffold) with a reported IC_{50} value of 2.1 μM, 2-phenylthiophene derivatives[17,18] (IC_{50} ranging from 0.11 to 0.97 μM), and the

Received: August 16, 2024
Revised: October 31, 2024
Accepted: November 26, 2024

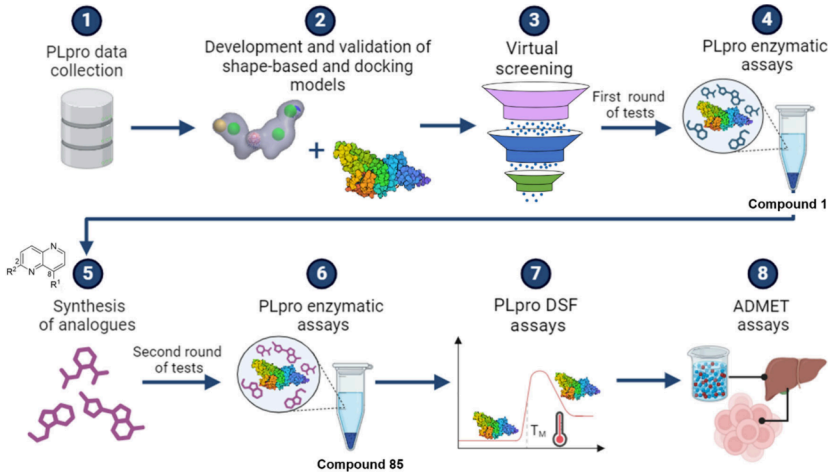

Figure 1. Integrated computational and experimental workflow applied for the discovery of novel noncovalent inhibitors of SARS-CoV-2 PLpro.

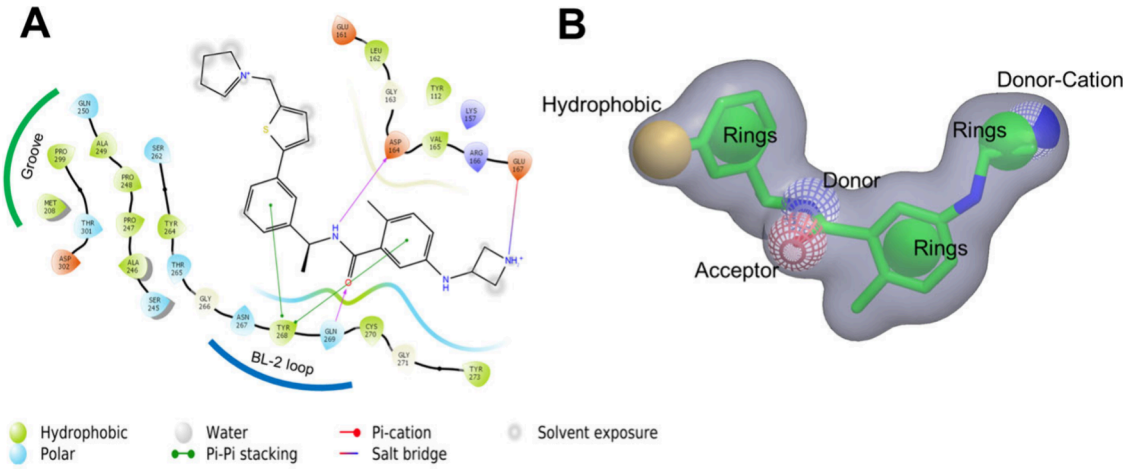

Figure 2. (A) 2D diagram of interactions of compound XR8-24 (BL2-Loop binding inhibitor) with PLpro residues of BL2-Loop. (B) Best shape-based model using the XR8-24 PLpro inhibitor as a template.

Table 1. Statistical Metrics Were Obtained for the PLpro Shape-Based Model[a]

		TOP 1%		TOP 5%		TOP 10%	
query	AUC	EF	BEDROC	EF	BEDROC	EF	BEDROC
XR8-24-7	0.952	29.06	0.68	13.97	0.69	8.52	0.75

[a]AUC, area under the ROC curve; EF, enrichment factor; BEDROC, Boltzmann-enhanced discrimination of ROC.

RI173 compound[19] (dimorpholine-thiuram disulfide scaffold) with an IC_{50} of 0.2 μM. More recently, SIMR30301, an octahydroindolo[2,3-*a*]quinolizine analogue,[20] was discovered with an IC_{50} of 0.0399 μM. Another 85 biarylphenyl benzamide noncovalent PLpro inhibitors[21] were identified that inhibited PLpro with K_i values from 13.2 to 88.2 nM. Among them, the lead compound Jun12682 inhibited the protease, deubiquitinase, and deISGylase activity of PLpro. *In vivo* experiments confirmed Jun12682's activity against SARS-CoV-2, and its variants, and has proved it to be a promising oral SARS-CoV-2 antiviral candidate. Despite all efforts, there are still no approved drugs against SARS-CoV-2 targeting PLpro.

In this work, we have developed, validated, and applied computational approaches such as shape-based models, molecular docking, and similarity clustering as part of an integrated virtual screening campaign. Our primary goal was to strategically identify promising compounds from the Holistic Drug Discovery and Development Centre (H3D) in-house chemical library. The prioritized compounds represented diverse chemotypes, which were experimentally assessed for their potential as inhibitors of PLpro. From the most potent hit of the first round of compounds tested, an optimized naphthyridine series was synthesized and experimentally evaluated through enzymatic, differential scanning fluorimetry (DSF) and early absorption, distribution, metabolism, excretion, and toxicity (ADMET) assays. The general workflow is illustrated in Figure 1.

In order to perform the virtual screening (VS), the first step was to extensively collect data on PLpro inhibitors from the available literature to develop shape-based models (the first filter of the VS). This resulted in the identification of 63 PLpro active compounds. Shape-based models were then built to distinguish between active and inactive compounds against the SARS-CoV-2 PLpro. At the time of the literature survey, the most potent

https://doi.org/10.1021/acsmedchemlett.4c00420
ACS Med. Chem. Lett. XXXX, XXX, XXX−XXX

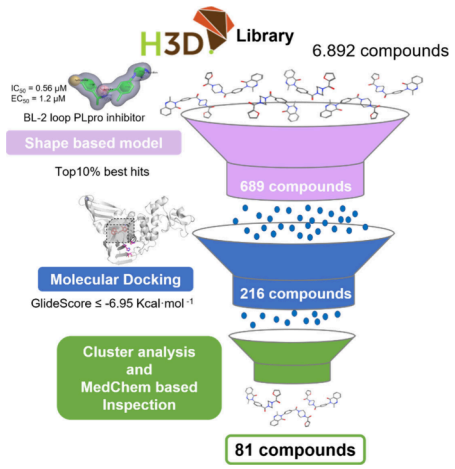

Figure 3. Schematic representation of the virtual screening workflow applied for the prioritization of potential candidates against SARS-CoV-2 PLpro.

PLpro noncovalent inhibitor described was XR8-24, with an IC_{50} of 0.56 μM,[21] and was selected as the core template for developing the shape-based models. The data set of XR8-24 derivatives was originally designed through a rational analysis (structure−activity relationship (SAR)) of a series of naphthalene scaffolds known for their activity against SARS-CoV-1 PLpro, despite their low metabolic stability in *in vivo* assays.[22−24] As a result, the best model (Figure 2) presented the following key interactions with PLpro: two aromatic benzene rings (involved in $\pi-\pi$ stacking interactions with the BL-2 loop Tyr268 residue), one hydrophobic thiophene (interacting with the hydrophobic "Groove" residues), one H-bond acceptor/donor amide group (interacting with the Asp164 and Gln269 residues), and one donor-cation (protonated azetidine) group (interacting with the Glu167 residue).

To validate the shape-based model, we gathered data on 14 inactive compounds against PLpro. We then simulated experimental conditions similar to those in a high-throughput screening campaign and generated 2254 decoys, which were added to the data set alongside the 14 inactive compounds from the literature.

The generated model achieved strong validation metrics, including an area under the ROC curve (AUC) of 0.95, an enrichment factor (EF) of 8.52, and a Boltzmann-enhanced discrimination of ROC (BEDROC) of 0.75, accurately identifying the top 10% of the tested data set from the literature (Table 1). Consequently, this shape-based model was employed as a filter during the virtual screening campaign.

Molecular docking calculations were performed with the Glide program[25−27] to predict the ligands binding mode and to filter candidates during the virtual screening. The ligands were obtained from the H3D in-house library, and the 3D structure of SARS-CoV-2 PLpro was obtained from the Protein Data Bank[28] (PDB ID 7LBS[18]). In order to assess the docking model reliability, we conducted the validation using the same data set collected and prepared from shape-based models, along with the crystal structure of SARS-CoV-2 PLpro PDB ID 7LBS.[18] The results obtained from the top 10% of the list revealed satisfactory metrics, an AUC of 0.96, EF of 9.21, and BEDROC of 0.77, justifying the utilization of the protocol developed for docking purposes (Supporting Information Figure S1).

The H3D database (6892 compounds) underwent screening using the most effective SARS-CoV-2 PLpro shape-based model, resulting in the filtration of the top 10% of the list, comprising 689 compounds. Subsequently, docking calculations were performed, applying a threshold of GlideScore ≤ -6.95 kcal·mol^{-1} (filtering to 216 compounds). Then, a cluster analysis based on chemical similarity and a medicinal chemistry (MedChem)-based inspection allowed the selection of 81 compounds (Supporting Information File 2) with good scores. These 81 compounds presented important interactions with residues of the BL-2 Loop and warranted prioritization for experimental evaluation (Figure 3).

The 81 compounds were evaluated *in vitro* for their inhibitory effects on PLpro, and nine of them exhibited some level of promising activity (Supporting Information Table S1). Among these, compound **1** showed an IC_{50} value of 73.60 ± 11.94 μM in the PLpro enzymatic assay (Figure 4A). In an inhibition test carried out with or without 0.01% Triton (Figure 4B), no significant differences were observed in the PLpro enzymatic activity, suggesting that this compound is not an aggregator. Kinetic characterization further suggested a competitive inhibition profile for **1**, with a K_i of 22.40 ± 6.7 μM, highlighting a moderate affinity for the target enzyme (Figure 4C). GRL0617 was used as a positive control for the enzymatic assays (Supporting Information Figure S2).

Considering the activity of **1**, a series of 30 naphthyridines were synthesized to explore the structure−activity relationships (SAR) between this naphthyridine chemical series and PLpro enzyme, with the goal of optimizing the inhibitor interactions with the PLpro enzyme and ultimately improving the SARS-CoV-2 antiviral activity (Supporting Information File 3). The 2,8-disubstituted-1,5-naphthyridines were synthesized using a linear synthetic route to allow diversification at the 2- and 8-positions of the naphthyridine core.[29,30] Scheme 1 (Supporting

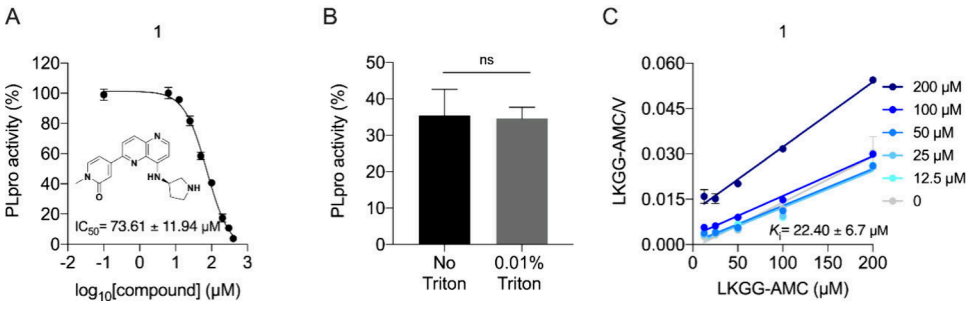

Figure 4. (A) Dose−response curve of **1** in the SARS-CoV-2 PLpro enzymatic activity. (B) Inhibition test of **1** in the absence and presence of 0.01% Triton. (C) Hanes−Woolf plot of compound **1**.

https://doi.org/10.1021/acsmedchemlett.4c00420
ACS Med. Chem. Lett. XXXX, XXX, XXX−XXX

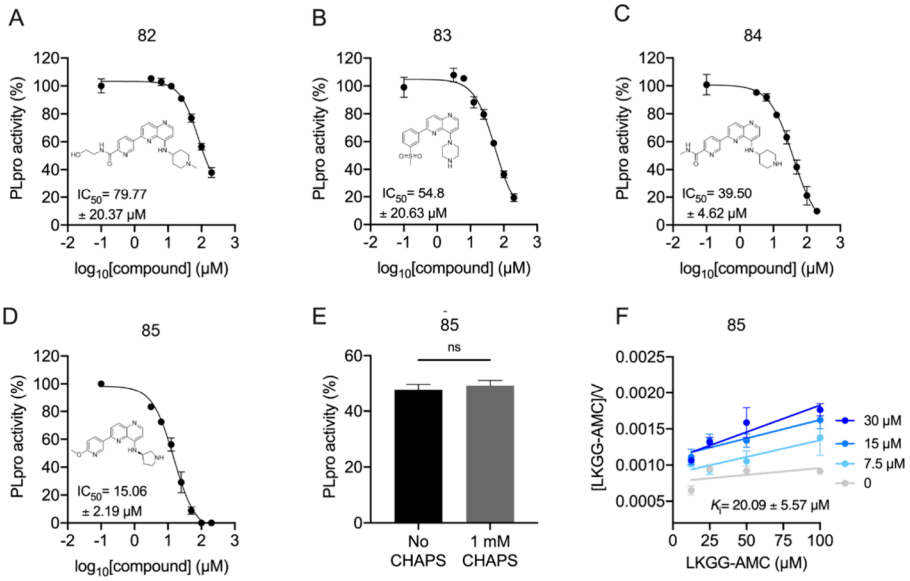

Figure 5. PLpro enzymatic assays for the selected compounds. (A, B, C, and D) Dose−response curves of compounds **82**, **83**, **84**, and **85**, respectively, in the SARS-CoV-2 PLpro enzymatic activity. (E) Compound **85** inhibition test in the absence and presence of 1 mM CHAPS detergent. (F) Hanes−Woolf plots of compound **85**.

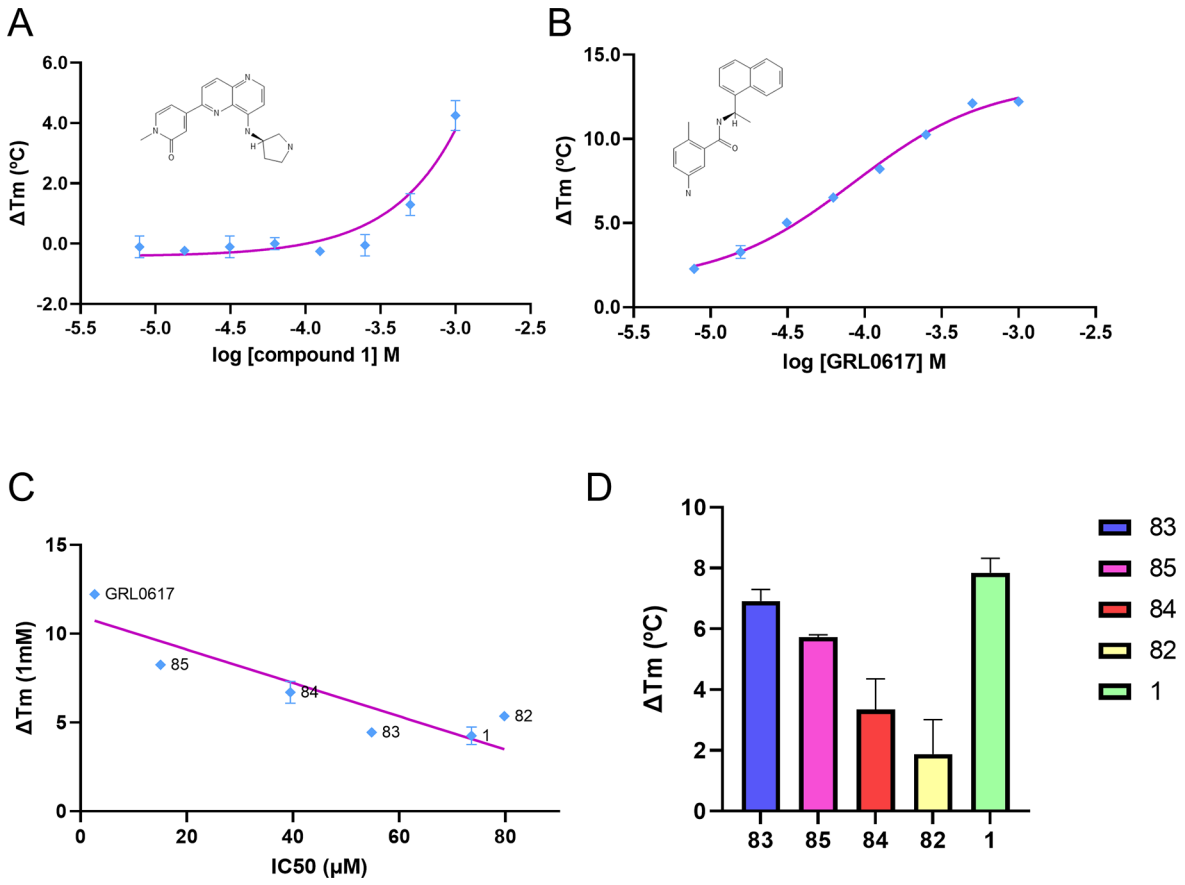

Figure 6. Differential scanning fluorimetry (DSF) analysis displaying the dose−response curve for compound **1** (A) compared to the noncovalent inhibitor GRL-0617 (B), which serves as a positive control. The *x* axis indicates the compound concentration (log *M*), while the *y* axis illustrates the thermoshift (°C). Panel C shows the correlation between potency, as measured by IC_{50} values (μM), and the corresponding thermoshift (°C) from biochemical assays. Last, panel D presents a bar graph depicting the single-dose thermoshift (ΔT_m) for compounds **1**, **82**, **83**, **84**, and **85**. Error bars represent the standard deviation of the measurements, providing insight into the reproducibility and reliability of the data.

Information) shows the synthetic procedure utilized for the analogues of **1**.

All 30 synthesized naphthyridine analogues were screened in a second round of PLpro enzymatic assays. The four most potent compounds, **82**, **83**, **84**, and **85**, presented PLpro IC_{50} values

https://doi.org/10.1021/acsmedchemlett.4c00420
ACS Med. Chem. Lett. XXXX, XXX, XXX−XXX

Table 2. *In Vitro* Enzymatic and ADMET Results for Selected Naphthyridine Analogues

		IC_{50} (μM)	CC_{50}(μM)		ADMET	
Compound	Chemical structure	PLpro	Vero	HepG2	Aqueous solubility (μM)	Microsomal stability (%)[a]
1	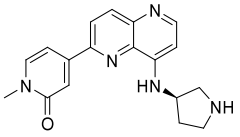	73.60 ± 11.94	23.77	>50	195	98.01/>99/94.35
82	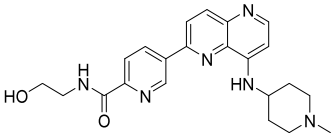	79.77 ± 20.37	>50	>50	200	95.54/97.35/94.22
83	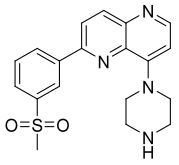	54.8 ± 20.63	43.58	>50	180	55.15/60.24/50.41
84	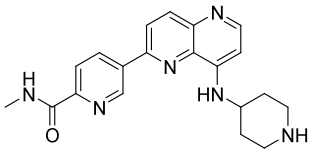	39.5 ± 4.62	47.32	>50	175	94.43/93.41/97.36
85	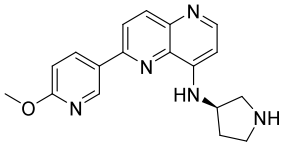	15.06 ± 2.19	7.47	26.33	190	54.64/66.61/62.68

[a]% remaining after 30 min, human/mouse/rat. Data from Kandepedu and collaborators.[29]

ranging from 15.06 to 79.77 μM (Figure 5A−D), respectively. For the most potent compound **85**, we performed an inhibition test with and without 1 mM of 3-((3-cholamidopropyl) dimethylammonio)-1-propanesulfonate (CHAPS) detergent to verify whether the inhibition was due to aggregation. No significant difference was observed (Figure 5E). As observed for the initial hit **1**, compound **85** showed a competitive inhibition mechanism with a K_i of 22.93 ± 6.41 μM (Figure 5F).

The results of differential scanning fluorimetry (DSF) for the single-dose assays for **1** and its derivatives (Figure 6A−D) illustrate that changes in melting temperature are induced by the compounds. Notably, all compounds exhibited a thermoshift greater than 1 °C, indicating their binding to the PLpro protein. To further validate the specificity of these interactions, dose−response assays were conducted. The graphical representations of these assays show that compound **1** and its derivatives produce a clear dose−response curve, confirming specific interactions with the PLpro protein when compared to the positive control, GLR0617 (Figure 6B). Additionally, upon comparison of the outcomes derived from both enzymatic and DSF assays, an observable correlation emerges between the potency of compounds and their corresponding thermoshift (Figure 6C). This correlation can be leveraged to optimize the compound screening process.

The results of the *in vitro* aqueous solubility, cytotoxicity, and microsomal stability properties of the five most promising naphthyridine derivatives (compounds **1**, **82**, **83**, **84**, and **85**) are presented in Table 2. All compounds exhibited high aqueous solubility (175−200 μM), which is beneficial for potential oral administration and crucial for bioavailability.

All five naphthyridine compounds were evaluated for cytotoxicity against two mammalian cell lines, namely, Vero and HepG2, respectively (Table 2). The two most potent PLpro inhibitors (compounds **1** and **85**) demonstrated 2−3-fold higher toxicity against the Vero cell line (CC_{50} = 23.77 and 7.47 μM, respectively) and compounds **83** and **84** were equipotent against Vero cells. On the other side, all compounds demonstrated weaker toxicity against HepG2, indicating a more favorable safety profile against the human cell line. The difference in cytotoxicity observed between HepG2 and Vero cells can be attributed to the distinct biological characteristics of these two cell lines. HepG2 cells are derived from human liver carcinoma and possess more efficient detoxification mechanisms, including cytochrome P450 enzymes, which may metabolize or neutralize toxic compounds. In contrast, Vero cells are derived from monkey kidney epithelial cells and lack many of the metabolic pathways found in liver cells.[31−33] As a result, compounds that are nontoxic to HepG2 cells may

https://doi.org/10.1021/acsmedchemlett.4c00420
ACS Med. Chem. Lett. XXXX, XXX, XXX−XXX

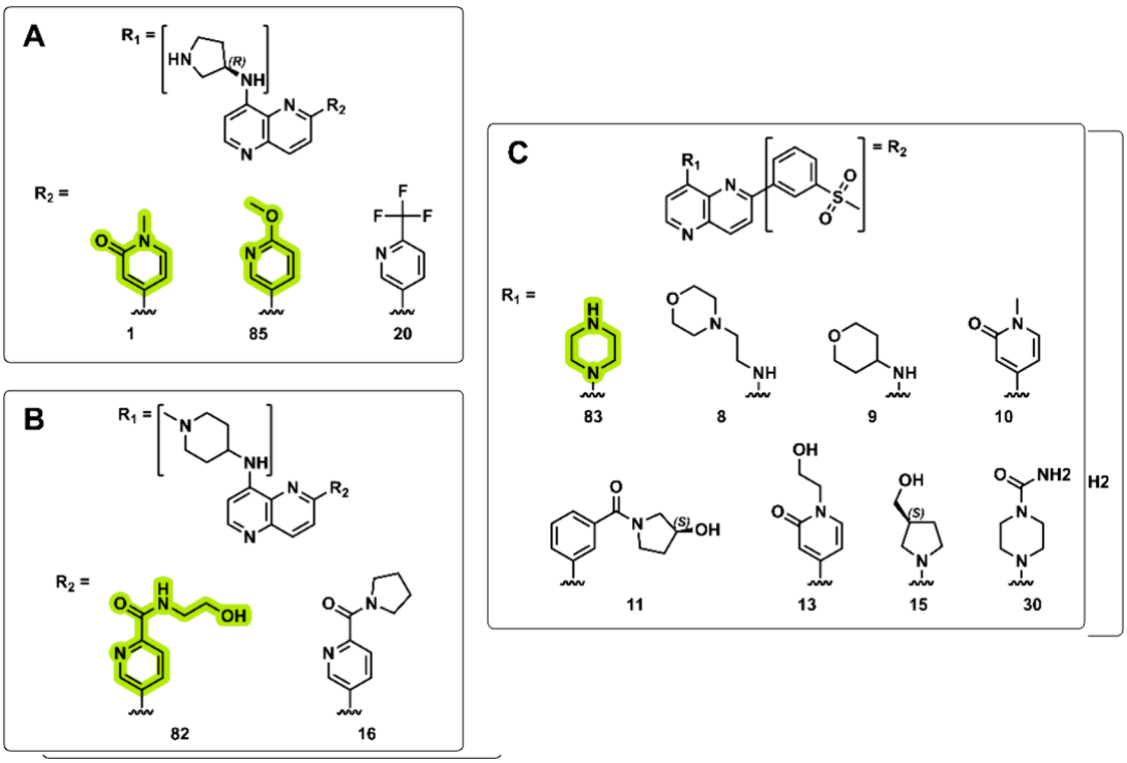

Figure 7. SAR analysis of naphthyridine derivatives. (A) R_1 = (3*R*)-3-aminopyrrolidin-1-yl group with exploration at R_2. (B) R_1 = (1-methylpiperidin-4-yl)aminyl group with exploration at R_2. (C) R_2 = 4-methanesulfonylphenyl with exploration at R_1. Substituents that rendered favorable improvements in PLpro IC_{50} are highlighted in green.

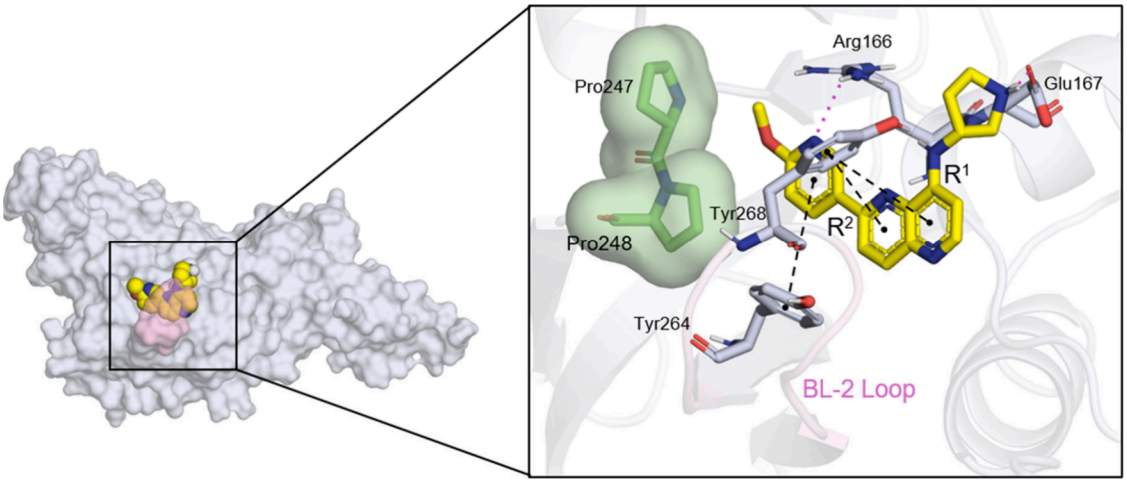

Figure 8. Docking pose of compound **85**, the most promising inhibitor of SARS-CoV-2 PLpro identified in this study, along with its ligand−protein interactions. On the left, the papain-like protease (PLpro) is illustrated using a blue-white surface representation, with the BL-2 loop highlighted in light pink and the ligand shown as yellow spheres. The right panel provides a zoomed-in view of the ligand−protein interactions, featuring a green surface to indicate hydrophobic interactions, pink dashed lines representing hydrogen bonds, and black dashed lines denoting $\pi-\pi$ stacking interactions. This detailed visualization underscores the binding characteristics of compound **85** and its potential as an effective therapeutic agent.

accumulate to toxic levels in Vero cells, leading to cytotoxic effects. This disparity underscores the importance of using different cell lines to assess cytotoxicity, as it helps capture a broader range of potential toxic responses in varying cellular environments.[32] Future SAR studies should include efforts to understand and diverge the PLpro activity and cytotoxicity relationship.

Microsomal stability was tested in human, mouse, and rat liver microsomes over a 30 min period (Table 2). Compounds retaining over 50% of their initial concentration after 30 min are considered to have good metabolic stability, with ideal stability being over 85%. Compounds **1**, **82**, and **84** demonstrated high metabolic stability across the mouse, rat, and human liver microsomes, with more than 90% of the compound remaining after 30 min. In contrast, compounds **83** and **85** showed lower stability, particularly against human microsomes, with only about 50% remaining.

When the data in Table 2 for compounds **1** and **85** are reviewed, the replacement of the 1-methylpyridin-2(1H)-one with 2-methoxypyridine led to a 5-fold improvement in PLpro

https://doi.org/10.1021/acsmedchemlett.4c00420
ACS Med. Chem. Lett. XXXX, XXX, XXX−XXX

activity but at a cost to metabolic stability in human, rat, and mouse liver microsomes. This may be due to an increased susceptibility to demethylation of the methoxy substituent in the presence of microsomes. In comparison, compound **83**'s apparent loss in metabolic stability in microsomes appears to be attributed to the piperazinyl group. To better understand the metabolic fate of compounds **83** and **85**, liquid chromatography-tandem mass spectrometry (LC-MS/MS) metabolic identification (MetID) could be done in future work to identify the metabolites. Further SAR expansion at these positions would also provide valuable information to understand the metabolic fate for the series.

In this study, an initial SAR exploration was carried out for this series by keeping the naphthyridine core constant and exploring diverse substituents at the 8′- (R_1) and 2′- (R_2) positions on the naphthyridine core (Figure 7).

When R_1 is a 3-aminopyrrolidinyl group, the substitution of R_2 with a pyridone (**1**) or methoxypyridine group (**85**; Figure 7A) resulted in IC_{50} values of 73.60 and 15.06 μM, respectively. This 5-fold improvement in PLpro activity may be the result of a more optimal orientation of the pyridinyl-*N* (moving from the 4′ to 3′ position) and the increase of the electron donating character of the *N*, which enhances the proposed interaction with the Arg166 residue (Figure 8). This can be further validated by comparison with **20** where the highly electron-withdrawing *ortho*-trifluoromethyl group would significantly reduce the electron-donating character of the pyridinyl-*N*. This would compromise the key electron-donating interaction with Arg166, which could potentially predict and agree with the observed complete loss in PLpro activity. The pyrrolidine ring at R_1 of compound **85** interacts with Glu167 through both a hydrogen bond and a salt bridge (Figure 8), as predicted by docking calculations. At R_2, a 6-methoxypyridine interacts by accepting a hydrogen from Arg166, and the ring engages in π-stacking interactions with Tyr264. In contrast, the 1-methyl-2-oxo-1,2-dihydropyridin-4-yl substituent (compound **1**) is more polar and exhibits reduced aromaticity due to the partial conjugation of the ring caused by the oxo group. This disruption seems to weaken its interaction with the enzyme's active site, leading to a higher IC_{50} (73.60 μM). Compound **85** also presents interaction with Glu167 (Figure 8). The flexibility in R_2 maintains hydrophobic interactions with the BL-2 loop. On the other hand, substituents such as 6-(trifluoromethyl)pyridin-3-yl (**20**; Figure 7A), despite its high lipophilicity and electronegative character, showed no activity.

Where R_1 is a (1-methylpiperidin-4-yl)aminyl group, substituting R_2 with a 6-[(2-hydroxyethyl)carbamoyl]pyridin-3-yl (**82**; Figure 7B) resulted in moderate activity (IC_{50} of 79.77 μM) against the PLpro enzyme. This substituent is more polar and sterically bulky and may impact its ability to make the key hydrophobic interactions with the enzyme (Supporting Information Figure S3). Similarly to **85**, the pyridinyl-*N* is in the proposed more favored 3′-position, which could lead to the weak retention of PLpro activity. In contrast, the substitution of R_2 with 6-[(2-hydroxyethyl)carbamoyl]pyridin-3-yl (**16**; Figure 7B) at the same position resulted in no measurable activity. This moiety is more lipophilic and rigid, which may hinder binding through polar interactions.

While retaining R_2 as a 4-methanesulfonylphenyl group, the substitution of R_1 with a piperazin-1-yl (**83**; Figure 7C) was favorable, yielding an IC_{50} of 54.81 μM. Similar to compounds **1**, **82**, and **85**, a basic group at position R_1 that is able to make the key salt bridge interactions with the PLpro Glu167 residue (Supporting Information Figure S3) is critical for activity. In contrast, nonbasic substituents that are not able to make the critical salt-bridge interaction with Glu167 at the same position, such as (oxan-4-yl)aminyl (**9**), (1-methyl-2-oxo-1,2-dihydropyridin-4-yl)methyl (**10**), 3-[(3S)-3-hydroxycyclopentanecarbonyl]phenyl (**11**), [1-(2-hydroxyethyl)-2-oxo-1,2-dihydropyridin-4-yl]-methyl (**13**), (3R)-3-(hydroxymethyl)-pyrrolidin-1-yl (**15**), and 4-carbamoyl-piperazin-1-yl (**30**; Figure 7C), did not exhibit any activity. For **8**, the increased steric bulk and altered electronic environment due to the oxygen in the morpholine ring may contribute to the lack of activity. These findings provide valuable insights into the structural elements that either contribute to or hinder the inhibitory effects of the compound on PLpro.

In conclusion, our integrated approach that combined computational strategies and experimental validation unveiled a novel class of noncovalent naphthyridine inhibitors of the SARS-CoV-2 PLpro enzyme. From 81 prioritized virtual hits of the H3D database, we identified the naphthyridine compound **1** that exhibited moderate activity against PLpro. The limited structural optimization of this compound led to the identification of compound **85** with increased potency against PLpro. Moreover, the naphthyridine series exhibited promising ADMET profiles with high aqueous solubility and high to moderate microsomal stability. Cytotoxicity was identified as a possible concern to developability of the naphthyridine series as a treatment for SARS-CoV-2. Future work should include SAR exploration to understand the observed unfavorable enzymatic vs cytotoxicity relationship and identify SAR trends that could diverge the series enzymatic activity from the cytotoxicity. Overall, these findings provide a foundation for the continued exploration of the naphthyridine scaffold as a potential antiviral therapeutic agent in future hit-to-lead optimization efforts. The discovery of noncovalent inhibitors of SARS-CoV-2 PLpro provides new mechanistic insights into the inhibition of this critical viral enzyme. Understanding these interactions at the molecular level can guide the design of more potent and selective inhibitors. Moreover, given the conserved nature of PLpro across different coronaviruses, the inhibitors identified in this study could potentially be effective against a broad spectrum of coronaviruses including those that may emerge in the future.

■ ASSOCIATED CONTENT

Data Availability Statement

The data curation script utilized in this study is available at https://github.com/LabMolUFG/cheminformatics_pipeline.

Supporting Information

The Supporting Information is available free of charge at https://pubs.acs.org/doi/10.1021/acsmedchemlett.4c00420.

Detailed computational procedures, chemical structures of the 30 naphthyridines, experimental procedures, supplementary figures, and compounds' characterizations (PDF)

Data for compunds 1−81 (XLSX)

Chemical structures (XLSX)

■ AUTHOR INFORMATION

Corresponding Author

Carolina Horta Andrade − *Center for the Research and Advancement in Fragments and Molecular Targets (CRAFT), Faculdade de Cîencias Farmaceuticas de Ribeirão Preto, Universidade de São Paulo, Ribeirão Preto, São Paulo 05508-*

https://doi.org/10.1021/acsmedchemlett.4c00420
ACS Med. Chem. Lett. XXXX, XXX, XXX−XXX

070, Brazil; Laboratory for Molecular Modeling and Drug Design (LabMol), Faculdade de Farmácia and Center for Excellence in Artificial Intelligence (CEIA), Instituto de Informática, Universidade Federal de Goiás, Goiânia, Goiás 74690-900, Brazil; orcid.org/0000-0003-0101-1492; Email: carolina@ufg.br

Authors

Bruna K. P. Sousa − *Center for the Research and Advancement in Fragments and Molecular Targets (CRAFT), Faculdade de Ciências Farmaceuticas de Ribeirão Preto, Universidade de São Paulo, Ribeirão Preto, São Paulo 05508-070, Brazil; Laboratory for Molecular Modeling and Drug Design (LabMol), Faculdade de Farmácia, Universidade Federal de Goiás, Goiânia, Goiás 74690-900, Brazil*

Melina Mottin − *Center for the Research and Advancement in Fragments and Molecular Targets (CRAFT), Faculdade de Ciências Farmaceuticas de Ribeirão Preto, Universidade de São Paulo, Ribeirão Preto, São Paulo 05508-070, Brazil; Laboratory for Molecular Modeling and Drug Design (LabMol), Faculdade de Farmácia, Universidade Federal de Goiás, Goiânia, Goiás 74690-900, Brazil; Pathogen-Host Interface Laboratory, Department of Cell Biology, University of Brasilia, Brasilia 73345-010, Brazil*

Donald Seanego − *Holistic Drug Discovery and Development Centre (H3D), University of Cape Town, Cape Town 7701, South Africa*

Christopher D. Jurisch − *Holistic Drug Discovery and Development Centre (H3D), University of Cape Town, Cape Town 7701, South Africa*

Beatriz S. A. Rodrigues − *Pathogen-Host Interface Laboratory, Department of Cell Biology, University of Brasilia, Brasilia 73345-010, Brazil*

Verônica L. S. da Silva − *Pathogen-Host Interface Laboratory, Department of Cell Biology, University of Brasilia, Brasilia 73345-010, Brazil*

Milene Aparecida Andrade − *Pathogen-Host Interface Laboratory, Department of Cell Biology, University of Brasilia, Brasilia 73345-010, Brazil*

Gilberto S. Morais Junior − *Pathogen-Host Interface Laboratory, Department of Cell Biology, University of Brasilia, Brasilia 73345-010, Brazil*

Diogo F. Boerin − *Center for the Research and Advancement in Fragments and Molecular Targets (CRAFT), Faculdade de Ciências Farmaceuticas de Ribeirão Preto and Laboratório de Cristalografia de Proteínas, Faculdade de Ciências Farmacêuticas de Ribeirão Preto, Universidade de São Paulo, Ribeirão Preto, São Paulo 05508-070, Brazil*

Thamires Q. Froes − *Center for the Research and Advancement in Fragments and Molecular Targets (CRAFT), Faculdade de Ciências Farmaceuticas de Ribeirão Preto and Laboratório de Cristalografia de Proteínas, Faculdade de Ciências Farmacêuticas de Ribeirão Preto, Universidade de São Paulo, Ribeirão Preto, São Paulo 05508-070, Brazil*

Flávia Nader Motta − *Pathogen-Host Interface Laboratory, Department of Cell Biology, University of Brasilia, Brasilia 73345-010, Brazil; Faculdade de Ceilândia, Universidade de Brasília, Brasília, Distrito Federal 73345-010, Brazil*

M. Cristina Nonato − *Center for the Research and Advancement in Fragments and Molecular Targets (CRAFT), Faculdade de Ciências Farmaceuticas de Ribeirão Preto and Laboratório de Cristalografia de Proteínas, Faculdade de Ciências Farmacêuticas de Ribeirão Preto, Universidade de São Paulo, Ribeirão Preto, São Paulo 05508-070, Brazil*

Izabela D. M. Bastos − *Pathogen-Host Interface Laboratory, Department of Cell Biology, University of Brasilia, Brasilia 73345-010, Brazil*

Kelly Chibale − *Holistic Drug Discovery and Development Centre (H3D), South African Medical Research Council Drug Discovery and Development Research Unit, and Institute of Infectious Disease and Molecular Medicine, University of Cape Town, Cape Town 7701, South Africa;* orcid.org/0000-0002-1327-4727

Richard K. Gessner − *Holistic Drug Discovery and Development Centre (H3D), University of Cape Town, Cape Town 7701, South Africa*

Complete contact information is available at: https://pubs.acs.org/10.1021/acsmedchemlett.4c00420

Author Contributions

¶B.K.P. Sousa, M. Mottin, and D. Seanego contributed equally to this work. Each author has contributed significantly to this work. C.H.A. and R.K.G. coordinated, designed, and supervised the project. C.H.A., M.C.N., I.D.M.B., and K.C. acquired funding for this project. B.K.P.S. and M.M. performed the computational experiments. D.S. and C.D.J. synthesized the compounds and organized the synthetic and structure elucidation experimental data. B.S.A.R., F.N.M., and I.D.M.B. provided biochemical enzymatic data. D.F.B., T.Q.F., and M.C.N. performed the SARS-CoV-2 PLpro DSF assays. B.K.P.S. organized the data and wrote the first draft of the manuscript. M.M. and D.S. further refined the manuscript. All authors read, edited, and contributed to the final version of the manuscript.

Funding

This work has been funded by CNPq BRICS STI COVID-19 (#441038/2020-4), FAPEG (#202010267000272), São Paulo Research Foundation (FAPESP grants #2020/06190-0, #2021/10084-3, #2021/13237-5, and #2020/05369-6). C.H.A., M.C.N., and I.D.M.B. are CNPq research fellows. D.F.B. was supported by a fellowship from FAPESP (2022/15854-4). B.K.P.S. was supported by a fellowship from Brazilian agency CNPq (process 142059/2020-0). The South African Medical Research Council (SAMRC) and Strategic Innovation Partnerships (SHIP) unit of the SAMRC are acknowledged for their financial support (K.C.). The Article Processing Charge for the publication of this research was funded by the Coordination for the Improvement of Higher Education Personnel - CAPES (ROR identifier: 00x0ma614).

Notes

The authors declare no competing financial interest.

■ ACKNOWLEDGMENTS

We are grateful to ChemAxon (https://chemaxon.com/), OpenEye Scientific Software Inc. (https://www.eyesopen.com/), and Pymol (The PyMOL Molecular Graphics System, Version 2.0 Schrödinger, LLC) for providing academic licenses of their software. The authors thank Monica Clements, Sauvik Samanta, Jasmin Ferreira, and Godwin Dziwornu for contributing to the synthesis of the naphthyridine compounds at H3D (University of Cape Town). We further thank Dale Taylor, Mathew Njoroge, and Keabetswe Masike from H3D (University of Cape Town) for their technical assistance with the *in vitro* ADME and cytotoxicity assays. We finally recognize John

Woodland at H3D for his efforts in helping secure funding for this project and useful discussions. The authors would also like to express their gratitude to Prof. Josué de Moraes (Research Center for Neglected Diseases at Guarulhos University, SP, Brazil) for his invaluable discussions concerning the cytotoxicity results.

■ ABBREVIATIONS

3CLpro, 3C-like protease; ACE2, angiotensin-converting enzyme 2; ADMET, absorption, distribution, metabolism, excretion, and toxicity; AUC, area under the curve; BEDROC, Boltzmann-enhanced discrimination of receiver operating characteristic; BL-2, binding loop 2; CHAPS, 3-((3-cholamidopropyl) dimethylammonio)-1-propanesulfonate; COVID-19, coronavirus disease 2019; DMSO, dimethyl sulfoxide; DSF, differential scanning fluorimetry; EC_{50}, 50% effective concentration; EF, enrichment factor; IC_{50}, half maximal inhibitory concentration; K_i, inhibition constant; LC-MS/MS, liquid chromatography-tandem mass spectrometry; MedChem, medicinal chemistry; MetID, metabolic identification; Mpro, main protease; NSP, nonstructural proteins; PDB, Protein Data Bank; PLpro, papain-like protease; SARS-CoV-2, severe acute respiratory syndrome coronavirus 2; VS, virtual screening; WHO, World Health Organization

■ REFERENCES

(1) Msemburi, W.; Karlinsky, A.; Knutson, V.; Aleshin-Guendel, S.; Chatterji, S.; Wakefield, J. The WHO Estimates of Excess Mortality Associated with the COVID-19 Pandemic. *Nature* **2023**, *613* (7942), 130−137.

(2) *Centers for Disease Control and Prevention, Vaccines for COVID-19 | CDC*. https://www.cdc.gov/coronavirus/2019-ncov/vaccines/index.html (accessed Nov 4, 2021).

(3) Karim, S. S. A.; Karim, Q. A. Omicron SARS-CoV-2 Variant: A New Chapter in the COVID-19 Pandemic. *Lancet* **2021**, *398* (10317), 2126−2128.

(4) Owen, D. R.; Allerton, C. M. N.; Anderson, A. S.; Aschenbrenner, L.; Avery, M.; Berritt, S.; Boras, B.; Cardin, R. D.; Carlo, A.; Coffman, K. J.; Dantonio, A.; Di, L.; Eng, H.; Ferre, R. A.; Gajiwala, K. S.; Gibson, S. A.; Greasley, S. E.; Hurst, B. L.; Kadar, E. P.; Kalgutkar, A. S.; Lee, J. C.; Lee, J.; Liu, W.; Mason, S. W.; Noell, S.; Novak, J. J.; Obach, R. S.; Ogilvie, K.; Patel, N. C.; Pettersson, M.; Rai, D. K.; Reese, M. R.; Sammons, M. F.; Sathish, J. G.; Singh, R. S. P.; Steppan, C. M.; Stewart, A. E.; Tuttle, J. B.; Updyke, L.; Verhoest, P. R.; Wei, L.; Yang, Q.; Zhu, Y. An Oral SARS-CoV-2 Mpro Inhibitor Clinical Candidate for the Treatment of COVID-19. *Science (80-.)* **2021**, *374* (6575), 1586−1593.

(5) Beigel, J. H.; Tomashek, K. M.; Dodd, L. E.; Mehta, A. K.; Zingman, B. S.; Kalil, A. C.; Hohmann, E.; Chu, H. Y.; Luetkemeyer, A.; Kline, S.; Lopez de Castilla, D.; Finberg, R. W.; Dierberg, K.; Tapson, V.; Hsieh, L.; Patterson, T. F.; Paredes, R.; Sweeney, D. A.; Short, W. R.; Touloumi, G.; Lye, D. C.; Ohmagari, N.; Oh, M.; Ruiz-Palacios, G. M.; Benfield, T.; Fätkenheuer, G.; Kortepeter, M. G.; Atmar, R. L.; Creech, C. B.; Lundgren, J.; Babiker, A. G.; Pett, S.; Neaton, J. D.; Burgess, T. H.; Bonnett, T.; Green, M.; Makowski, M.; Osinusi, A.; Nayak, S.; Lane, H. C. Remdesivir for the Treatment of Covid-19 — Final Report. *N. Engl. J. Med.* **2020**, *383* (19), 1813−1826.

(6) Grein, J.; Ohmagari, N.; Shin, D.; Diaz, G.; Asperges, E.; Castagna, A.; Feldt, T.; Green, G.; Green, M. L.; Lescure, F.-X.; Nicastri, E.; Oda, R.; Yo, K.; Quiros-Roldan, E.; Studemeister, A.; Redinski, J.; Ahmed, S.; Bernett, J.; Chelliah, D.; Chen, D.; Chihara, S.; Cohen, S. H.; Cunningham, J.; D'Arminio Monforte, A.; Ismail, S.; Kato, H.; Lapadula, G.; L'Her, E.; Maeno, T.; Majumder, S.; Massari, M.; Mora-Rillo, M.; Mutoh, Y.; Nguyen, D.; Verweij, E.; Zoufaly, A.; Osinusi, A. O.; DeZure, A.; Zhao, Y.; Zhong, L.; Chokkalingam, A.; Elboudwarej, E.; Telep, L.; Timbs, L.; Henne, I.; Sellers, S.; Cao, H.; Tan, S. K.; Winterbourne, L.; Desai, P.; Mera, R.; Gaggar, A.; Myers, R. P.; Brainard, D. M.; Childs, R.; Flanigan, T. Compassionate Use of Remdesivir for Patients with Severe Covid-19. *N. Engl. J. Med.* **2020**, No. NEJMoa2007016.

(7) Teoh, S. L.; Lim, Y. H.; Lai, N. M.; Lee, S. W. H. Directly Acting Antivirals for COVID-19: Where Do We Stand? *Front. Microbiol.* **2020**, *11*, DOI: 10.3389/fmicb.2020.01857.

(8) WHO Solidarity Trial Consortium. Repurposed Antiviral Drugs for Covid-19 — Interim WHO Solidarity Trial Results. *N. Engl. J. Med.* **2021**, *384* (6), 497−511.

(9) Sheahan, T. P.; Sims, A. C.; Zhou, S.; Graham, R. L.; Pruijssers, A. J.; Agostini, M. L.; Leist, S. R.; Schäfer, A.; Dinnon, K. H.; Stevens, L. J.; Chappell, J. D.; Lu, X.; Hughes, T. M.; George, A. S.; Hill, C. S.; Montgomery, S. A.; Brown, A. J.; Bluemling, G. R.; Natchus, M. G.; Saindane, M.; Kolykhalov, A. A.; Painter, G.; Harcourt, J.; Tamin, A.; Thornburg, N. J.; Swanstrom, R.; Denison, M. R.; Baric, R. S. An Orally Bioavailable Broad-Spectrum Antiviral Inhibits SARS-CoV-2 in Human Airway Epithelial Cell Cultures and Multiple Coronaviruses in Mice. *Sci. Transl. Med.*. **2020**, *12* (541), DOI: 10.1126/scitranslmed.abb5883.

(10) Agostini, M. L.; Pruijssers, A. J.; Chappell, J. D.; Gribble, J.; Lu, X.; Andres, E. L.; Bluemling, G. R.; Lockwood, M. A.; Sheahan, T. P.; Sims, A. C.; Natchus, M. G.; Saindane, M.; Kolykhalov, A. A.; Painter, G. R.; Baric, R. S.; Denison, M. R. Small-Molecule Antiviral *β*- D-N4-Hydroxycytidine Inhibits a Proofreading-Intact Coronavirus with a High Genetic Barrier to Resistance. *J. Virol.* **2019**, *93* (24), DOI: 10.1128/JVI.01348-19.

(11) Tan, H.; Hu, Y.; Jadhav, P.; Tan, B.; Wang, J. Progress and Challenges in Targeting the SARS-CoV-2 Papain-like Protease. *J. Med. Chem.* **2022**, *65* (11), 7561−7580.

(12) Ratia, K.; Saikatendu, K. S.; Santarsiero, B. D.; Barretto, N.; Baker, S. C.; Stevens, R. C.; Mesecar, A. D. Severe Acute Respiratory Syndrome Coronavirus Papain-like Protease: Structure of a Viral Deubiquitinating Enzyme. *Proc. Natl. Acad. Sci. U. S. A.* **2006**, *103* (15), 5717−5722.

(13) Ratia, K.; Kilianski, A.; Baez-Santos, Y. M.; Baker, S. C.; Mesecar, A. Structural Basis for the Ubiquitin-Linkage Specificity and DeISGylating Activity of SARS-CoV Papain-Like Protease. *PLoS Pathog.* **2014**, *10* (5), No. e1004113.

(14) Ghosh, A. K.; Brindisi, M.; Shahabi, D.; Chapman, M. E.; Mesecar, A. D. Drug Development and Medicinal Chemistry Efforts toward SARS-Coronavirus and Covid-19 Therapeutics. *ChemMedChem.* **2020**, *15* (11), 907−932.

(15) Rut, W.; Lv, Z.; Zmudzinski, M.; Patchett, S.; Nayak, D.; Snipas, S. J.; El Oualid, F.; Huang, T. T.; Bekes, M.; Drag, M.; Olsen, S. K. Activity Profiling and Crystal Structures of Inhibitor-Bound SARS-CoV-2 Papain-like Protease: A Framework for Anti−COVID-19 Drug Design. *Sci. Adv.* **2020**, *6* (42), DOI: 10.1126/sciadv.abd4596.

(16) Fu, Z.; Huang, B.; Tang, J.; Liu, S.; Liu, M.; Ye, Y.; Liu, Z.; Xiong, Y.; Zhu, W.; Cao, D.; Li, J.; Niu, X.; Zhou, H.; Zhao, Y. J.; Zhang, G.; Huang, H. The Complex Structure of GRL0617 and SARS-CoV-2 PLpro Reveals a Hot Spot for Antiviral Drug Discovery. *Nat. Commun.* **2021**, *12* (1), 488.

(17) Shen, Z.; Ratia, K.; Cooper, L.; Kong, D.; Lee, H.; Kwon, Y.; Li, Y.; Alqarni, S.; Huang, F.; Dubrovskyi, O.; Rong, L.; Thatcher, G. R.; Xiong, R. Potent, Novel SARS-CoV-2 PLpro Inhibitors Block Viral Replication in Monkey and Human Cell Cultures. *bioRxiv Prepr. Serv. Biol.* **2021**, *3*, 2021.02.13.431008.

(18) Shen, Z.; Ratia, K.; Cooper, L.; Kong, D.; Lee, H.; Kwon, Y.; Li, Y.; Alqarni, S.; Huang, F.; Dubrovskyi, O.; Rong, L.; Thatcher, G. R. J.; Xiong, R. Design of SARS-CoV-2 PLpro Inhibitors for COVID-19 Antiviral Therapy Leveraging Binding Cooperativity. *J. Med. Chem.* **2022**, *65* (4), 2940−2955.

(19) Meewan, I.; Kattoula, J.; Kattoula, J. Y.; Skinner, D.; Fajtová, P.; Giardini, M. A.; Woodworth, B.; McKerrow, J. H.; Lage de Siqueira-Neto, J.; O'Donoghue, A. J.; Abagyan, R. Discovery of Triple Inhibitors of Both SARS-CoV-2 Proteases and Human Cathepsin L. *Pharmaceuticals* **2022**, *15* (6), 744.

(20) Hersi, F.; Sebastian, A.; Tarazi, H.; Srinivasulu, V.; Mostafa, A.; Allayeh, A. K.; Zeng, C.; Hachim, I. Y.; Liu, S.-L.; Abu-Yousef, I. A.; Majdalawieh, A. F.; Zaher, D. M.; Omar, H. A.; Al-Tel, T. H. Discovery

https://doi.org/10.1021/acsmedchemlett.4c00420
ACS Med. Chem. Lett. XXXX, XXX, XXX−XXX

of Novel Papain-like Protease Inhibitors for Potential Treatment of COVID-19. *Eur. J. Med. Chem.* **2023**, *254*, No. 115380.
(21) Tan, B.; Zhang, X.; Ansari, A.; Jadhav, P.; Tan, H.; Li, K.; Chopra, A.; Ford, A.; Chi, X.; Ruiz, F. X.; Arnold, E.; Deng, X.; Wang, J. Design of a SARS-CoV-2 Papain-like Protease Inhibitor with Antiviral Efficacy in a Mouse Model. *Science (80-.)* **2024**, *383* (6690), 1434−1440.
(22) Sanders, B. C.; Pokhrel, S.; Labbe, A. D.; Mathews, I. I.; Cooper, C. J.; Davidson, R. B.; Phillips, G.; Weiss, K. L.; Zhang, Q.; O'Neill, H.; Kaur, M.; Schmidt, J. G.; Reichard, W.; Surendranathan, S.; Parvathareddy, J.; Phillips, L.; Rainville, C.; Sterner, D. E.; Kumaran, D.; Andi, B.; Babnigg, G.; Moriarty, N. W.; Adams, P. D.; Joachimiak, A.; Hurst, B. L.; Kumar, S.; Butt, T. R.; Jonsson, C. B.; Ferrins, L.; Wakatsuki, S.; Galanie, S.; Head, M. S.; Parks, J. M. Potent and Selective Covalent Inhibition of the Papain-like Protease from SARS-CoV-2. *Nat. Commun.* **2023**, *14* (1), 1733.
(23) Shan, H.; Liu, J.; Shen, J.; Dai, J.; Xu, G.; Lu, K.; Han, C.; Wang, Y.; Xu, X.; Tong, Y.; Xiang, H.; Ai, Z.; Zhuang, G.; Hu, J.; Zhang, Z.; Li, Y.; Pan, L.; Tan, L. Development of Potent and Selective Inhibitors Targeting the Papain-like Protease of SARS-CoV-2. *Cell Chem. Biol.* **2021**, *28* (6), 855−865.e9.
(24) Osipiuk, J.; Azizi, S.-A.; Dvorkin, S.; Endres, M.; Jedrzejczak, R.; Jones, K. A.; Kang, S.; Kathayat, R. S.; Kim, Y.; Lisnyak, V. G.; Maki, S. L.; Nicolaescu, V.; Taylor, C. A.; Tesar, C.; Zhang, Y.-A.; Zhou, Z.; Randall, G.; Michalska, K.; Snyder, S. A.; Dickinson, B. C.; Joachimiak, A. Structure of Papain-like Protease from SARS-CoV-2 and Its Complexes with Non-Covalent Inhibitors. *Nat. Commun.* **2021**, *12* (1), 743.
(25) *Glide*; Schrödinger, LLC: New York, 2019.
(26) Halgren, T. A.; Murphy, R. B.; Friesner, R. A.; Beard, H. S.; Frye, L. L.; Pollard, W. T.; Banks, J. L. Glide: A New Approach for Rapid, Accurate Docking and Scoring. 2. Enrichment Factors in Database Screening. *J. Med. Chem.* **2004**, *47* (7), 1750−1759.
(27) Friesner, R. a; Banks, J. L.; Murphy, R. B.; Halgren, T. a; Klicic, J. J.; Mainz, D. T.; Repasky, M. P.; Knoll, E. H.; Shelley, M.; Perry, J. K.; Shaw, D. E.; Francis, P.; Shenkin, P. S. Glide: A New Approach for Rapid, Accurate Docking and Scoring. 1. Method and Assessment of Docking Accuracy. *J. Med. Chem.* **2004**, *47* (7), 1739−1749.
(28) Berman, H. M.; Westbrook, J.; Feng, Z.; Gilliland, G.; Bhat, T. N.; Weissig, H.; Shindyalov, I. N.; Bourne, P. E. The Protein Data Bank. *Nucleic Acids Res.* **2000**, *28*, 235−242.
(29) Kandepedu, N.; Gonzàlez Cabrera, D.; Eedubilli, S.; Taylor, D.; Brunschwig, C.; Gibhard, L.; Njoroge, M.; Lawrence, N.; Paquet, T.; Eyermann, C. J.; Spangenberg, T.; Basarab, G. S.; Street, L. J.; Chibale, K. Identification, Characterization, and Optimization of 2,8-Disubstituted-1,5-Naphthyridines as Novel Plasmodium Falciparum Phosphatidylinositol-4-Kinase Inhibitors with in Vivo Efficacy in a Humanized Mouse Model of Malaria. *J. Med. Chem.* **2018**, *61* (13), 5692−5703.
(30) Dziwornu, G. A.; Seanego, D.; Fienberg, S.; Clements, M.; Ferreira, J.; Sypu, V. S.; Samanta, S.; Bhana, A. D.; Korkor, C. M.; Garnie, L. F.; Teixeira, N.; Wicht, K. J.; Taylor, D.; Olckers, R.; Njoroge, M.; Gibhard, L.; Salomane, N.; Wittlin, S.; Mahato, R.; Chakraborty, A.; Sevilleno, N.; Coyle, R.; Lee, M. C. S.; Godoy, L. C.; Pasaje, C. F.; Niles, J. C.; Reader, J.; van der Watt, M.; Birkholtz, L.-M.; Bolscher, J. M.; de Bruijni, M. H. C.; Coulson, L. B.; Basarab, G. S.; Ghorpade, S. R.; Chibale, K. 2,8-Disubstituted-1,5-Naphthyridines as Dual Inhibitors of Plasmodium Falciparum Phosphatidylinositol-4-Kinase and Hemozoin Formation with In Vivo Efficacy. *J. Med. Chem.* **2024**, *67*, 11401.
(31) Morais, C. S.; Mengarda, A. C.; Miguel, F. B.; Enes, K. B.; Rodrigues, V. C.; Espírito-Santo, M. C. C.; Siyadatpanah, A.; Wilairatana, P.; Couri, M. R. C.; de Moraes, J. Pyrazoline Derivatives as Promising Novel Antischistosomal Agents. *Sci. Rep.* **2021**, *11* (1), 23437.
(32) Dematei, A.; Nunes, J. B.; Moreira, D. C.; Jesus, J. A.; Laurenti, M. D.; Mengarda, A. C. A.; Vieira, M. S.; do Amaral, C. P.; Domingues, M. M.; de Moraes, J.; Passero, L. F. D.; Brand, G.; Bessa, L. J.; Wimmer, R.; Kuckelhaus, S. A. S.; Tomás, A. M.; Santos, N. C.; Plácido, A.; Eaton, P.; Leite, J. R. S. A. Mechanistic Insights into the Leishmanicidal and Bactericidal Activities of Batroxicidin, a Cathelicidin-Related Peptide from a South American Viper (Bothrops Atrox). *J. Nat. Prod.* **2021**, *84* (6), 1787−1798.
(33) Campelo, Y.; Ombredane, A.; Vasconcelos, A.; Albuquerque, L.; Moreira, D.; Plácido, A.; Rocha, J.; Hilarion Fokoue, H.; Yamaguchi, L.; Mafud, A.; Mascarenhas, Y.; Delerue-Matos, C.; Borges, T.; Joanitti, G.; Arcanjo, D.; Kato, M.; Kuckelhaus, S.; Silva, M.; De Moraes, J.; Leite, J. Structure−Activity Relationship of Piplartine and Synthetic Analogues against Schistosoma Mansoni and Cytotoxicity to Mammalian Cells. *Int. J. Mol. Sci.* **2018**, *19* (6), 1802.

https://doi.org/10.1021/acsmedchemlett.4c00420
ACS Med. Chem. Lett. XXXX, XXX, XXX−XXX